Investigation on fire resistance of steel-reinforced concrete-filled steel tubular columns subjected to non-uniform fire

Wen-Jing Mao[a], Kan Zhou[b], Wen-Da Wang[a]*

[a] *School of Civil Engineering, Lanzhou University of Technology, Lanzhou 730050, PR China*

[b] *School of Built Environment, Engineering and Computing, Leeds Beckett University, City Campus, Leeds, LS1 3HE, UK*

Abstract: The fire performance of steel-reinforced concrete-filled steel tubular (SRCFST) columns under non-uniform fire exposure is analytically and experimentally examined. Four SRCFST columns are methodically tested under 3-, 2-opposite-, 2-adjacent-, and 1-face heating to achieve the failure modes, temperature evolution in time, axial and lateral deformations, and fire resistance. Finite element (FE) analysis models were used to verify and assess the test results. The obtained results reveal that profiled steel benefits the integrity and fire resistance of SRCFST columns. The temperature distribution of the cross-section is substantially affected by uneven temperature distribution, resulting in shifting the stiffness center toward the unexposed side at the elevated temperature. The parametric studies are also conducted over various influential factors to analyze their effects on the fire resistance of SRCFST columns subjected to non-uniform fire. A modified calculation methodology based on the extended Rankine approach is developed to predict the fire resistance of SRCFST columns under various fire conditions, covering uniform fire, 3-, 2-opposite-, 2- adjacent-, and 1-face heating. Based on the quantitative comparisons between the experimentally observed data and the numerically predicted results, the simplified method generally yields accurate predictions on the ultimate load capacity of SRCFST columns under non-uniform fire.

Keywords: Steel-reinforced concrete-filled steel tubular (SRCFST) columns; Non-uniform fire; Thermo-mechanical behavior; Finite element (FE) model; Simplified design method.

*Corresponding author at: School of Civil Engineering, Lanzhou University of Technology, PR China

E-mail: wangwd@lut.edu.cn (W.-D. Wang).

1. Introduction

Steel-reinforced concrete-filled steel tubes (SRCFST), consisting of inner concrete, an encased steel section, and an outer steel tube, are rapidly gaining popularity in tall buildings and large-span structures. As a branch from concrete-filled steel tubes (CFST), it inherited the advantages of conventional CFST [1]. Extensive research on the mechanical performance of SRCFST columns is available in the last decade and mainly focused on the mechanical performance of stub columns under axial and bending loads, pure bending load, lateral shear load, combined compression and torsion, and lateral impact load [2-10]. The existing studies reveal that SRCFST columns exhibit the remarkable performance of load-carrying capacities and seismic performance compared to CFST columns. The ductility and strength of these columns were noticeably enhanced due to the reinforcements that the steel section provides to the inner concrete.

A building fire can lead to the failure or even collapse of the structure. The study of fire resistance performance as a crucial mechanical characteristic of the structure in service conditions has attracted much attention. SRCFST columns were also expected to perform well against fire. As previously reported, extensive experiments and numerical analyses have been conducted to examine the fire behavior of composite columns. The performed works mostly focused on conventional CFST columns subjected to uniform fire. For this purpose, slender columns with circular, square, rectangular, and elliptical cross-sections were tested under both axial and eccentric forces to estimate their fire resistance [11, 12]. The achieved results revealed that the fire resistance of elliptical CFST columns would be higher than that of rectangular columns with the same total steel ratio. The influence of the infilled concrete and steel tube strength on the fire resistance was experimentally estimated and compared with that of the CFST with normal strength [13-15]. The fire resistance of columns infilled with high-strength concrete under the high load level was reported to be lower than that of columns

filled with normal strength, although the load-bearing capacity at ambient temperature could be substantially enhanced. The fire response of CFST columns under various boundary restraints was also discussed by test and numerical calculations [16, 17]. The fiber beam-columns models and three-dimensional FE model were developed to further examine the mechanical behavior of CFST columns under the combined action of load and fire [18-21]. The fire resistance of concrete-filled cold-formed steel built-up (CF-CFS) columns were experimentally and numerically investigated [22-24]. The predicted fire resistance of CF-CFS columns using EN 1994-1-2 [25] were evaluated by Rahnavard et al. [22]. Additionally, various design approaches have been proposed to predict the fire resistance of CFST columns subjected to simultaneous load and uniform fire, as well as the ultimate bearing capacity after fire exposure [26-31].

Till now, a few investigations on the fire resistance of SRCFST columns have been conducted. Espinos et al. [32] explored the fire behavior of CFST columns and compared the obtained results with those of embedded circular hollow sections (i.e., double tube columns, profiled steel, and steel core) via FE analysis. The experimental investigations on fire resistance of CFST with embedded circular hollow sections and profiled steel were also performed by Chu et al. [33] and Yang et al. [34]. The test results and numerical simulations on the fire performance of CFST with embedded steel core were reported by Neuenschwander et al. [35, 36]. The FE-based model was employed by Tan et al. [37] to assess the fire resistance of steel-reinforced concrete-filled stainless steel tubular columns. The results for innovative CFST columns under the uniform fire indicated that all specimens exhibit overall buckling and failure in a relatively ductile manner due to the insertion of steel profiles. The exploitation of a double tube configuration was proved to be a good strategy for enhancing the fire behavior, followed by embedded profiled steel in CFST with the same total steel area. Further, the load redistribution among each component could be analyzed based on the time-histories of expansion,

and the load shared by profiled steel was reported to be magnified from 20.6% to 68.4% due to protection by concrete and outer steel tube [37]. Moreover, the compressive behavior of SRCFST stub columns after the fire exposure was experimentally examined, and the calculation methods for evaluating their ultimate bearing capacities were established by Yang et al. [38] and Meng et al. [39].

A careful literature survey generally reveled that existed investigations on the fire resistance of SRCFST columns chiefly focus on the cases that are acted upon by uniform fire. In real cases, columns are not always exposed to uniform fire attack and may be exposed to 1-, 2-opposite-, 2-adjacent-, and 3-face heating, depending on the position of the column in structures. The complexity and difference in temperature distribution and fire resistance of columns under non-uniform fire have been revealed through fire resistance tests on traditional CFST columns under 3- and 1-face heating [40-42] and numerical analyzes [43, 44]. The obtained results revealed that the boundary conditions pertinent to the non-uniform fire would have a substantial impact on the fire resistance and residual bearing capacity, and such effects would be lower for columns with more fire-exposed sides. Appropriate tests, including three SRCFST columns under the non-uniform fire and three specimens under the uniform fire for comparison purposes, were conducted by Meng et al. [45]. The achieved results indicated that the fire resistance of SRCFST columns subjected to 4- and 3-face heating would be almost similar, however, obvious different failure modes were detected. As above described, the non-uniform fire conditions offer a distinct influence on fire performance of SRCFST columns, and few reports and experimental data on SRCFST columns under non-uniform fire have been gathered, especially for cruciform steel-reinforced concrete-filled steel tubular columns subjected to 2-opposite-, 2-adjacent-face heating. Due to existence of embedded steel section, the fire resistance of SRCFST columns has significant improvement compared with that of CFST columns. It is questionable to directly apply the research achievement of conventional CFST columns to SRCFST

columns. Furthermore, design methods of conventional CFST columns are not applicable to SRCFST columns due to the remarkable contribution of profiled steel to fire resistance. Owing to insufficient test data and the absence of an inclusive design approach for SRCFST columns subjected to non-uniform fire, there is an urgent need to further realize fire performance and develop a design approach to assess their fire resistance.

This study is conducted to experimentally assess the fire resistance of SRCFST columns under the non-uniform fire, including 3-, 2-opposite-, 2-adjacent-, and 1-face heating, to enrich the test database. The test results for the above fire scenarios, their corresponding failure modes, temperature evolution in time, axial and lateral deformations, and fire resistance are comprehensively analyzed to reveal the fire behavior of SRCFST columns subjected to non-uniform fire. Additionally, numerical calculations are also conducted as supplementary experiments due to limitations on test parameters and expensive fire tests. By employing the developed FE-based model validated on the basis of the test results, inclusive parametric studies are performed to carefully explore the influence of various factors on the fire resistance. Finally, a modified calculation methodology based on the extended Rankine approach is further methodically constructed to capture the fire resistance of SRCFST columns under various fire conditions, including 4-, 3-, 2-opposite-, 2-adjacent-, and 1-face heating.

2. Testing programme

2.1 General description

Four square SRCFST column specimens under 3-, 2-opposite-, 2-adjacent-, and 1-face non-uniform fire are tested in the present investigation. The section sizes ($B \times t_s$) for the square hollow section are set as 300 mm × 5.5 mm, where t_s denotes the thickness of the steel tube, and B represents the edge length of the square steel tube. A cruciform profile labelled B is embedded in the core concrete for all understudied specimens. The specimen details and test variables are given in Table 1,

where SRCFST specimens are labelled to imply corresponding parameters. In this regard, “SS” denotes a square SRCFST specimen. The fire conditions are represented by “T” denoting three-face heating, and “O”, “B”, and “S” specify 2-opposite-, 2-adjacent-, and single-face heating cases, respectively. Furthermore, the used letter “U” indicates that the experimental scrutiny has been performed under the action of fire, and the letter “Z” represents the concentric loading, followed by the last number meaning the designed load level n. The load level is defined as a ratio of applied load during the fire test and ultimate bearing capacity at ambient temperature. The length of the column (L) is set equal to 3810 mm for all specimens, including two end plates of thickness 30 mm. The schematic representation details of SRCFST columns have been demonstrated in Fig. 1.

Table 1 Measured geometric dimensions of SRCFST column specimens

Specimen ID	Fire boundary	Load level, n	Applied load(kN)	Fire Resistance time, t_R (min)	Failure mode
SSTU-Z-50	3-sided	0.491	3000	70	Global+local bucking
SSOU-Z-50	2-opposite-sided	0.497	3037	88	Global+local bucking
SSBU-Z-50	2-adjacent-sided	0.514	3140	59	Global+local bucking
SSSU-Z-50	1-sided	0.507	3097	55	Global+local bucking

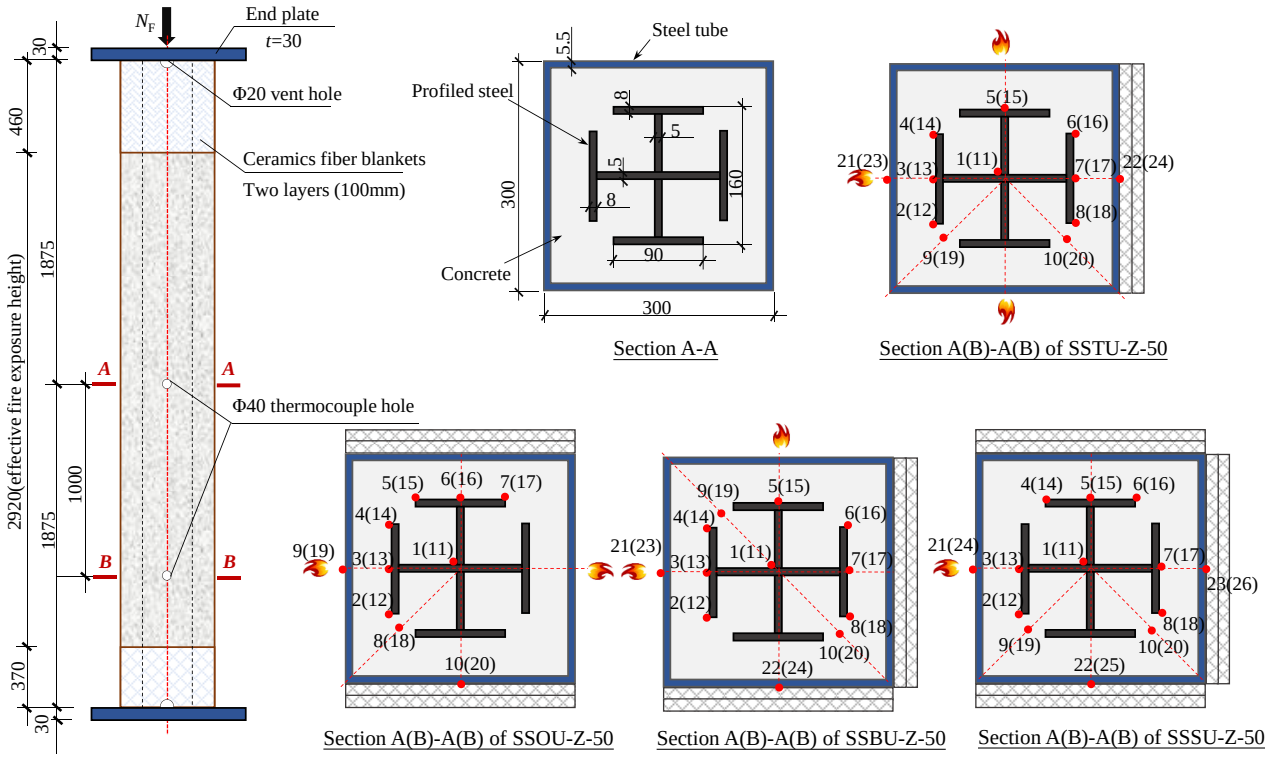

Fig.1 Test specimen design (unit: mm)

Four SRCFST specimens are fabricated in the same batch processing as SRCFST specimens

tested under the uniform fire, which is described in some detail in Ref. [46]. The specimens are installed with hinge supports at both ends.

Table 2 Material properties of steel at ambient temperature

Cross-section	E_s(GPa)	f_y(MPa)	f_u(MPa)	μ_s	δ_{10}(%)	f_y/f_u
Circular steel tube	193.04	345.02	455.17	0.29	35	0.76
squarer steel tube	181.44	325.55	458.58	0.29	41	0.71
Steel plane-5mm	174.49	276.59	419.74	0.29	37	0.66
Steel plane -8mm	154.63	260.79	412.37	0.29	40	0.63

The ambient-temperature mechanical properties of both the outer steel tube and embedded steel section are determined through tensile coupon tests according to specified codes. The key material properties at ambient temperature are summarized in Table 2. Ready-mixed concrete was employed for the fabrication of the test specimens. Standard cubic test blocks with a side of 150 mm were casted and cured together with the test specimens under the same condition. For the sake of brevity, the mix proportion of concrete has been reported in Ref. [46] in details. Therefore, the cube compressive tests were carried out at 28-day and the day of fire testing (155 days) at ambient temperature, and the corresponding averaged strength are 47.4 MPa and 64.4 MPa, respectively.

2.2 Instrumentation and test procedure

For the non-exposed surfaces, two layers of ceramic fiber blankets with a thickness of 50mm (add up to 100 mm) are tied to the external surface of the steel tube. Ceramic fiber blankets are fastened by a steel wire that can endure a temperature up to 1200 ℃. Type K thermocouples with a diameter of 3 mm are fitted within two cross-sections to measure and compare the temperature distribution. Some efforts are made to fit the tips of the thermocouples at the same location for these two cross-sections. The arrangement of the thermocouples has been presented in Fig. 1, where the numbers in parentheses indicate the measurement points arranged in section B-B.

Two vertical displacement gauges are attached to the top face of the top-end plate to measure the vertical deformation during the test. A horizontal gauge is also mounted outsides the furnace to

record the lateral deflection during the test. During installation, the specimens are aligned with the center of the hinge supports by high-strength bolts to apply axial load.

The fire tests are conducted in the vertical fire furnace at Southeast University, China. Sixteen gas burners and twenty-five thermocouples mounted on the furnace wall are employed to control and monitor the furnace temperature. The target load is applied and maintained for approximately 30 min to ensure that the axial deformation has been stabilized before heating is started. The furnace is designed to enable manual control at the start of heating and subsequent automatic control to ensure the furnace temperature follows the ISO-834 standard curve [47]. The fire tests are terminated when the specimens fail to carry the exerted load or the failure criterion is reached. The failure is commonly met in the following cases: (i) the axial deformation exceeds 0.01 H (mm); (ii) the deformation rate exceeds 0.003 H (mm/min), where H represents the height of fire exposure in meter [47]. The applied axial load is provided by the controlled hydraulic jack with a capacity of 5000 kN and is maintained constant during the whole fire exposure.

3. Analysis of results

3.1 Test observations

The failure modes of four specimens have been displayed in Fig. 2. Global buckling is detectable for all specimens, despite the difference in the fire exposure arrangements. The lateral deflections take their peak values near the mid-height of columns. The experimentally observed data reveals that outward local buckling of the steel tube in the compression region takes place, regularly distributed along the length of the columns.

The steel tube and profiled steel are cut open to observe the internal failure modes. Fig. 3 shows the internal failure mode of SSBU-Z-50. The steel tubes can be easily removed due to the relatively weak restraint of square steel tubes. Local crushing of concrete is observed in the compression zone. In addition, the transverse concrete cracks in the tensile zone which are mostly distributed near the

maximum lateral deformation, are also examined due to laterally flexural behavior. The slight shedding of the concrete surface is detected around the outward local buckling of the steel tube.

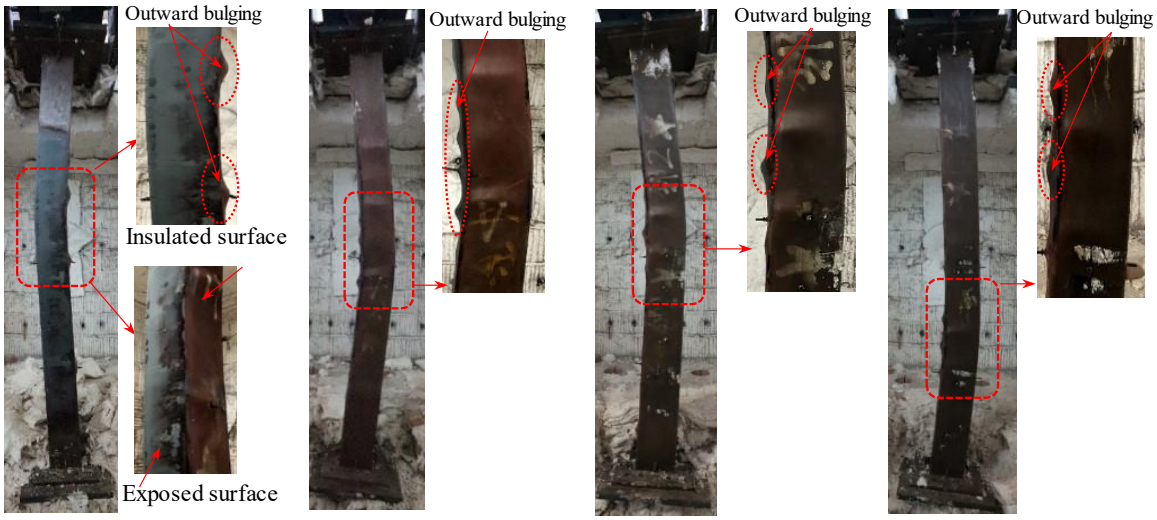

(a) SSTU-Z-50 (b) SSOU-Z-50 (c) SSBU-Z-50 (d) SSSU-Z-50

Fig.2 Failure modes of specimens after fire tests

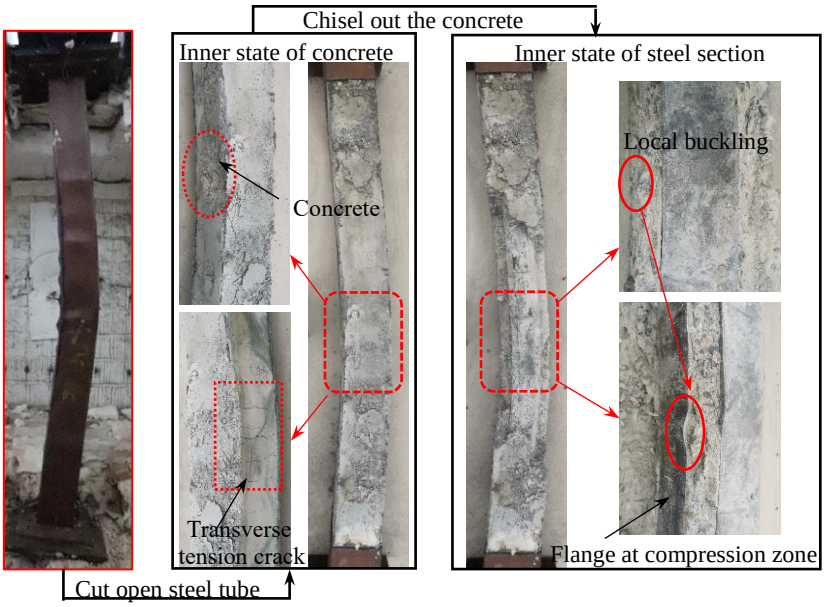

Fig.3 Inner failure modes of specimen SSBU-Z-50

Fig. 3 also demonstrates the failure mode of the steel section, which presented a similar flexural pattern with overall specimens. The obvious local buckling in the flange of profiled steel at the compression zone is observable. Due to the crackling of concrete under the action of external load, the bonding failure occurs at the interface of the concrete and the profiled steel flange. As expected, no visible detachment for profiled steel and concrete surrounded by profiled steel is detected,

indicating their appropriate composite action during the fire exposure. Therefore, the integrity and stability of profiled steel could be noticeably enhanced due to reinforcement action, as shown by concrete. The insertion of profiled steel and concrete surrounded by circular profiled steel provides a core area for bearing capacity during fire exposure. It is beneficial to the stiffness and bearing capacity of the SRCFST columns under the non-uniform fire.

3.2 Thermal response

The average furnace temperature and the temperature of four specimens have been plotted in Figs. 4-7. The furnace temperature is reasonably close to the ISO-834 fire curve for all tested specimens. Generally, the surface temperature obtained by the steel tube develops at a slower rising rate than that of the furnace temperature. For the measuring points of the steel tube on the exposed side, the temperature quickly increases to 600 ℃ within 40 min, resulting in severe degeneration of stiffness and strength. The temperature of the steel tube at the unexposed side is expectedly lower than that at the exposed side due to covering by ceramic fiber blankets with temperature discrepancies ranging from 150-400 ℃ at the end of fire exposure. The obtained results reveal that the temperature registered by measuring point 23 of specimen SSSU-Z-50 represents the lowest one at the same time because both two adjacent surfaces of point 23 are unexposed to fire.

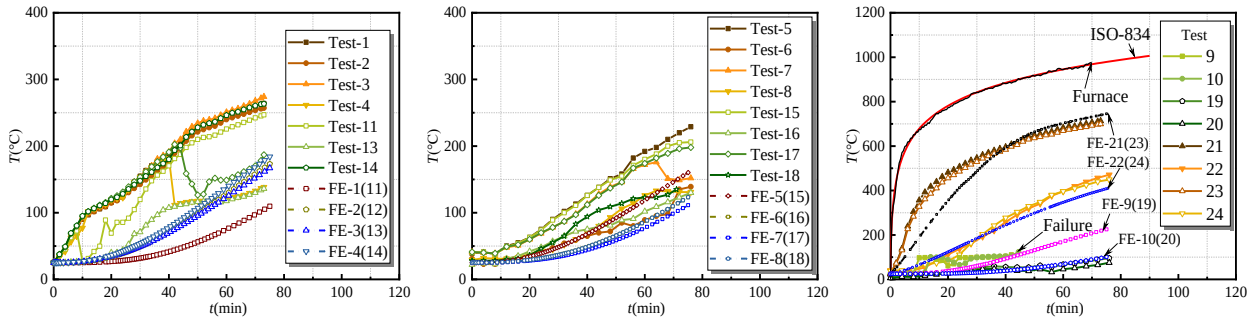

(a) (b) (c)

Fig.4 Temperature evolutions in time of specimen SSTU-Z-50 (a) Profiled steel measuring point near exposed side; (b) Profiled steel measuring point near unexposed side; (c) Steel tube and concrete measuring point

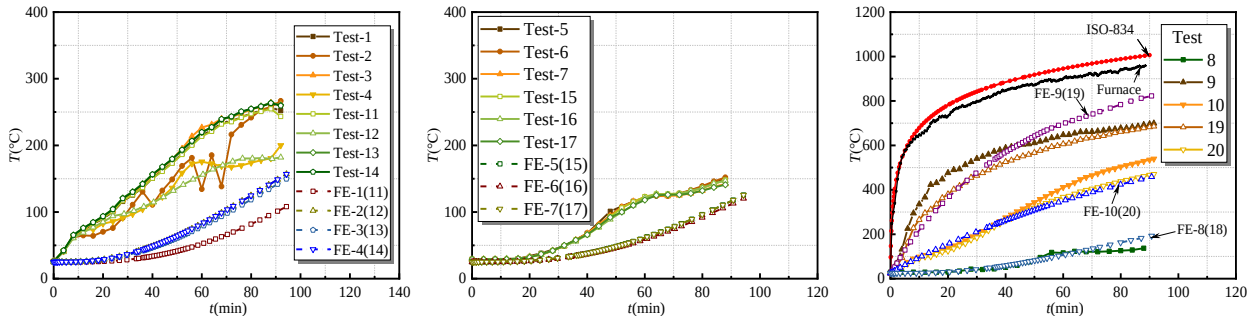

(a) (b) (c)

Fig.5 Temperature evolutions in time of specimen SSOU-Z-50 (a) Profiled steel measuring point near exposed side; (b) Profiled steel measuring point near unexposed side; (c) Steel tube and concrete measuring point

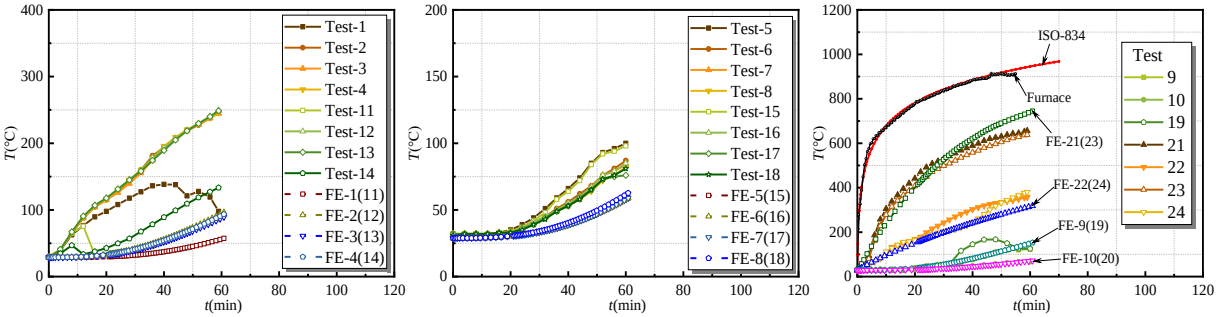

(a) (b) (c)

Fig.6 Temperature evolutions in time of specimen SSBU-Z-50 (a) Profiled steel measuring point near exposed side; (b) Profiled steel measuring point near unexposed side; (c) Steel tube and concrete measuring point

The temperature increasing inside the concrete is substantially lagging compared to the steel tube, observed a plateau or slow increase in temperature curves at about 100 ℃ caused by moisture migration after free water evaporation. Except for the specimen subjected to 2-opposite side fire, measuring point 9 (19) in concrete (closer to the exposed side) exhibits a higher temperature. For instance, the temperature of points 9 and 10 for specimen SSSU-Z-50 in order are 114 ℃ and 47 ℃. The temperature of profiled steel is developed at a slow rate caused by being surrounded by concrete. Similar to concrete, the temperature of the profiled steel near the exposed side is higher than those far away from the exposed side, while the whole temperature of the profiled steel remains below 300 ℃ after heating for 1.5 h. It further indicates that the region surrounded by profiled steel forms a core area with low temperatures. In other words, the degradation of material properties of the core area is limited, which is beneficial for the bearing capacity at a late period of fire exposure. Additionally, the temperature associated with the two-layer of thermocouples is graphically compared, proving that the

temperature has been uniformly distributed along the longitudinal direction of the columns.

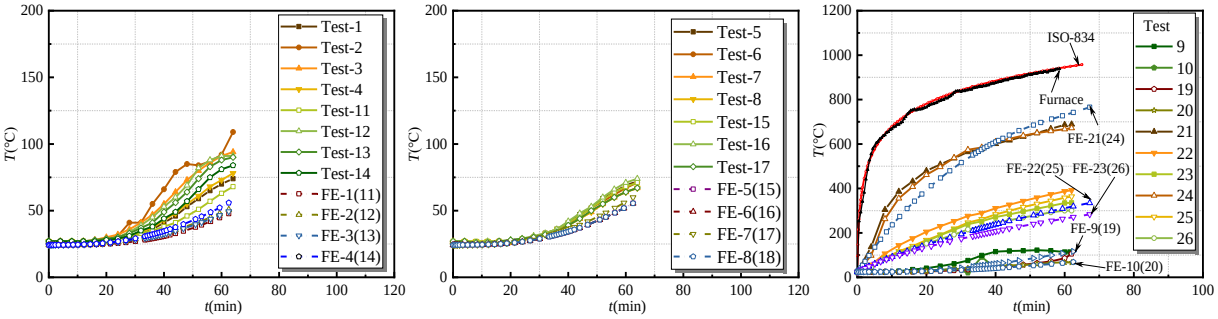

(a) (b) (c)

Fig.7 Temperature evolutions in time of specimen SSSU-Z-50 (a) Profiled steel measuring point near exposed side; (b) Profiled steel measuring point near unexposed side; (c) Steel tube and concrete measuring point

To further examine the influence of the non-uniform fire on the temperature gradient of the cross-section, the temperature distribution at the end of fire exposure has been plotted in Fig. 8. In this figure, the results for specimen SSOU-Z-50 have been excluded due to its symmetrical fire condition, in which *d* denotes the depth of the cross-section such that takes zero for the edge of measuring point 21. Apparent thermal gradients are detectable throughout the cross-sectional domain. For measuring points located at the same coordinates, those with more exposed sides exhibit higher temperatures. Furthermore, the lowest temperature regions are closer to the unexposed side, indicating the asymmetric temperature distribution along the center of the cross-section. The degradations of strength and stiffness are inconsonant at elevated temperature, revealing the eccentricity of cross-sectional strength. The achieved results indicate that the stiffness center gradually shifts toward the unexposed side with the rise of temperature for specimens under the non-uniform fire.

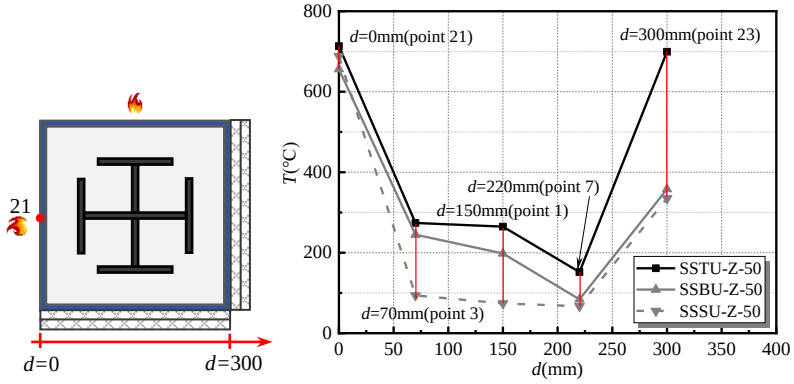

Fig.8 Temperature distribution of specimens along cross-section at the end of fire exposure

3.3 Deformation-time response

The deformation results of specimens under the non-uniform fire have been illustrated in Fig. 9. The demonstrated results show that all axial deformations developed in a similar trend such that thier corresponding curves could be divided into three stages (see Fig. 9(a)). At the early stage of fire exposure, the axial deformation is essentially dominated by the thermal expansion of the steel tube. Both the steel tube and profiled steel are welded with the top of the end plate, resulting in concordant axial deformation between them. Therefore, detachment at the interface of concrete and top-end plate could occur at this stage. The compression load is chiefly shared by the steel tube and embedded profiled steel until reaching the peaks of the expansion deformation. After that, the rate of contraction overcomes the rate of expansion due to the serious reduction of the stiffness and strength of the steel tube with rising temperature. The concrete is re-contacted with the upper endplate. The load shared by the profiled steel and concrete gradually enhances due to the load being redistributed. Finally, the contraction deformation abruptly increases until failure occurs.

In Fig. 9, the time-history plots of the axial and lateral deformations of SRCFST columns have been provided. For specimens under 2-opposite-, 2-adjacent-, and single-face heating, the lateral deformation at the compression side (exposed side) is appropriately measured, where the deflection toward the exposed side is considered with a negative sign. The displacement gauge measured lateral deformation of specimen SSTU-Z-50 is broken during the fire test, resulting in data failure. Similar to axial deformation, three obvious branches are detectable. Due to the asymmetric temperature distribution, heat-induced expansion continues to increase in the radial direction. The expansion rate of the exposed side is higher than that of the unexposed side in the initial stage. As a result, a deflection towards the exposed side in the column will be first generated, and subsequently, the deflection occurs in the opposite direction. The reason is the effect induced by the change of the stiffness center on the

lateral deformation, which overcomes the initial deflection induced by asymmetric thermal expansion. For test specimens under the 2-opposite-, 2-adjacent-, and single-face heating, it further indicates that the position of the external load is closer to the exposed side compared to the stiffness center in the presence of the non-uniform fire. This conclusion can be analyzed in the following.

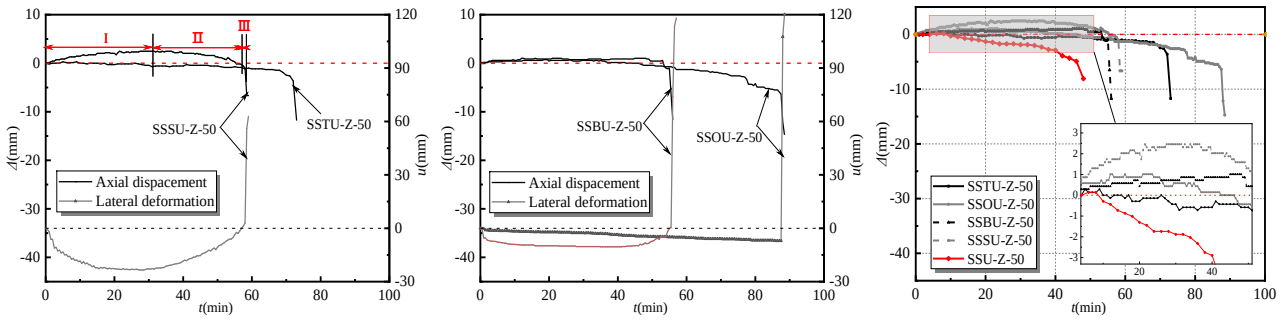

(a) SSTU-Z-50 and SSSU-Z-50 (b) SSBU-Z-50 and SSOU-Z-50 (c) Comparison on axial displacement-time curves

Fig.9 Deformation versus time relationships of SRCFST column specimens subjected to non-uniform fire

The axial deformation of specimen SSU-Z-50 exposed to uniform fire as reported in Ref. [46] is now compared with the present test results (see Fig. 9(c)). It is worth noting that the only difference in the test parameters of five SRCFST columns is the fire condition. The plotted results display that the overall axial deformation trend is consistent. The magnitude of peak expansion and reaching time magnify with the lessening of the exposed surfaces. Furthermore, the specimen SSSU-Z-50 undergoes a continuous overall expansion before the failure. This crucial fact is because the heat-induced expansion of specimens with more exposed sides is counteracted earlier with a contraction deformation induced by the externally applied load.

4. FE analysis and discussion

In this section, the FE models are developed by employing general-purpose ABAQUS software. Two types of models, namely, heat transfer analysis and mechanical analysis model, are successively established to conduct further explorations on the fire response of SRCFST columns. Meanwhile, the predicted results by the FE models are successfully validated with the experimental data in this paper,

followed by an in-depth analysis of the fire resistance under various fire conditions. Subsequently, a comprehensive parametric study is also conducted to reveal the roles of influential factors.

4.1 Development and validation of temperature field models

The four-node shell element DS4 is employed to simulate the thermal response of the steel tube and profiled steel, eight-node brick heat transfer element DC3D8 is adopted for concrete herein. The thermal properties of materials recommended in Eurocode 4 [25] are employed herein. These characteristics mainly include density, specific heat, and thermal conductivity. The moisture content of 5% (by weight) is assumed in specific heat of concrete to consider the moisture evaporation. The thermal convection coefficient and thermal emissivity coefficient of exposed sides are taken as 25 W/(m^2·℃) and 0.5, respectively [25]. For unexposed sides, the value of the coefficient of heat transfer by convection is set equal to 9 W/(m^2·°C) [48]. It is emphasized that the effect of heat transfer due to radiation is also considered in this value. A maximum element density of B/20 was selected based on the prior mesh sensitivity study to ensure sufficient calculation accuracy. The An air gap is generated across the interface between concrete and steel due to both concrete shrinkage and the difference in heat-induced expansion between concrete and steel. Therefore, the thermal resistance value of the interface of concrete and steel tube is set as 100 W/(m^2·K) [36]. In addition, the thermal resistance of the interface of the inner concrete and the profiled steel is neglected based on the recommendations of a previous study [49].

The heat transfer models are developed based on the above description to capture the temperature-time curves and verify the test results. The graphical comparisons indicate that there exists a rationally good agreement between the predicted temperature evolution curves and those of experiments for all specimens (see Figs. 4-7).

4.2 Development and validation of mechanical models

For the mechanical modeling of the problem, a four-node shell element S4R for steel and a three-dimensional eight-node brick element C3D8R for concrete are utilized. The main aim is to suitably simulate the mechanical responses of SRCFST columns. To accurately import the temperature of each integration point, the mesh density should be appropriately identified with those exploited in the heat transfer models.

"Surface-to-surface contact" is defined as the mechanical interactions between steel and concrete, and the inner surface of steel tube is selected as a "master surface". A hard contact and penalty approach are set to represent the normal attribute and behavior in a tangential direction, respectively, in which the friction coefficient at the interface of steel and concrete is set equal to 0.6. A "tie" property is defined as the contact surface between the end plate and the steel tube, and also the interface between the profiled steel and the end plate. The load mode and boundary conditions are consistent with those in the test. Load initial eccentricity of $L/1000$ is employed at the ends of columns to simulate the initial straightness imperfection [50].

The stress-strain relationships of steel at elevated temperatures, as provided by Lie [51], are employed here. Fig. 10 (a) presents the stress-strain curves of steel at different temperature. For concrete, the material properties are described by the concrete damage plastic (CDP) model in ABAQUS. Temperature-dependent constitutive model of concrete in compression proposed by Han [52], modified based on the constitutive relations at ambient temperature, are inputted into the CDP model. The stress-strain curves of concrete at elevated temperature are displayed in Fig. 10 (b), taking tested specimens in this paper as an example. It should be pointed out that the stress-strain model proposed by Han [52] was originally used for CFST columns, in which the confinement effect provided by outer steel tube to infilled concrete has been considered. For tensile behavior of concrete

at elevated temperature, the stress-strain relationship recommended by Hong and Varma [53] was employed in this study and expressed by the Eq. (1). Note that the peak tensile stress f_t' was defined as 9% of the compressive strength f_c'.

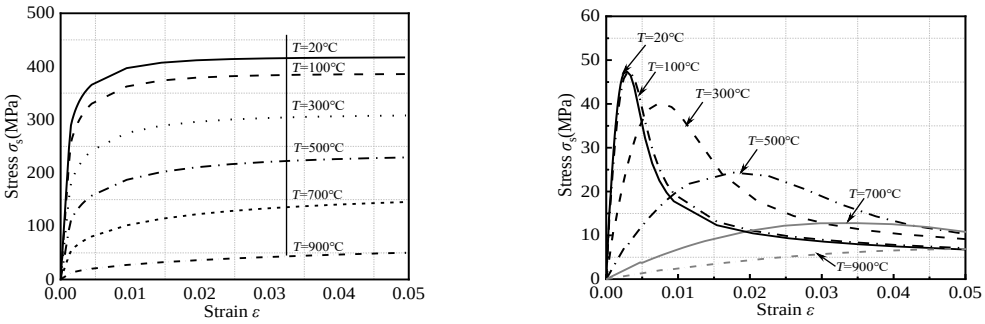

(a) (b)

Fig.10 Stress-strain curves for materials at elevated temperature (a) Q355 grade structural steel based on Lie [51]; (b) confinement concrete based on Han [52]

$$\sigma_{ct}=\begin{cases} E_c(T)\varepsilon & \varepsilon \le \varepsilon_{cr} \\ f_t'(T)-0.1f_t'(T)\dfrac{\varepsilon-\varepsilon_{cr}}{\varepsilon_{cr}} & \varepsilon_{cr}<\varepsilon \le 2\varepsilon_{cr} \\ 0.9f_t'(T) & \varepsilon \ge 2\varepsilon_{cr} \end{cases} \quad (1)$$

Based on the above explanations, the mechanical FE-based models are developed to simulate the mechanical response of test specimens, including axial deformation-time curves, fire resistance, and failure modes. Fig.11 presents the comparisons between predicted axial deformation curves and experimentally observed data in this work and Meng et al. [45]. In addition, the fire resistance of traditional CFST columns were also predicted and compared with experimental results [40, 41] (see Fig. 11 (d)-(f)). Moreover, the quantitative comparisons on the fire resistance are represented in Fig. 12.

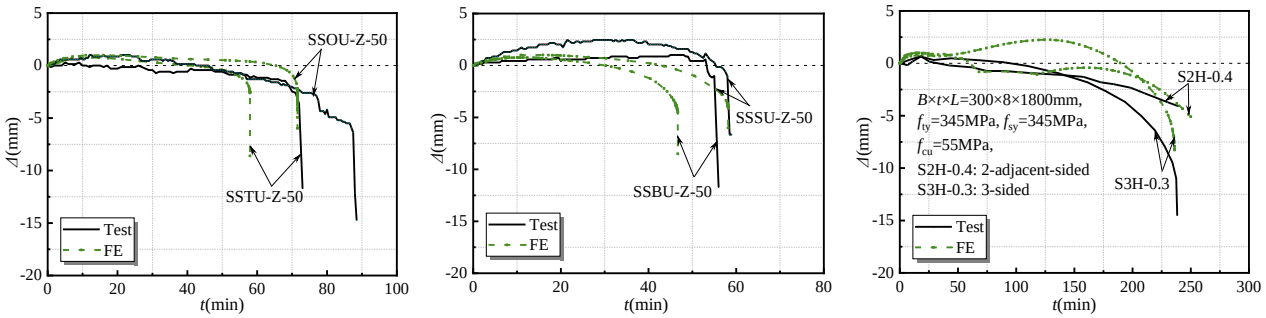

(a) SSTU-Z-50 and SSOU-Z-50 (b) SSBU-Z-50 and SSSU-Z-50 (c) SRCFST specimens tested by Meng et al. [45]

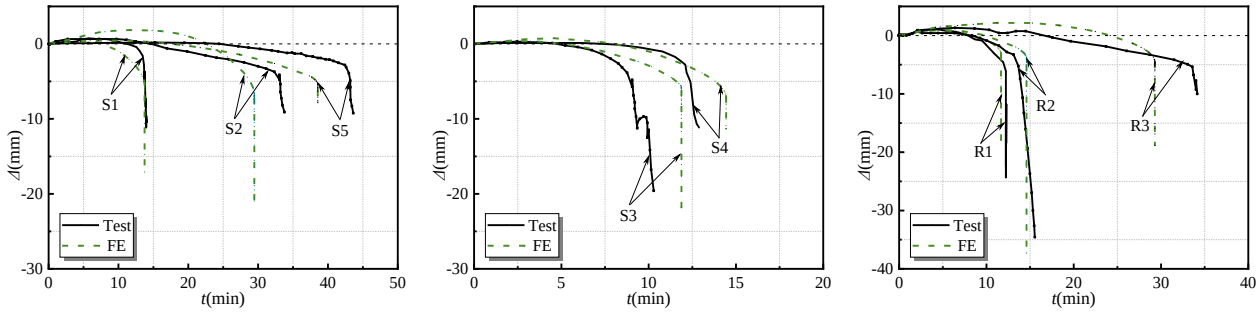

(d) CFST specimens S1, S2 and S5 [40] (e) CFST specimens S3 and S4 [40] (f) CFST specimens series R1-R3 [41]

Fig.11 Comparisons between the predicted and measured axial-deformation curves

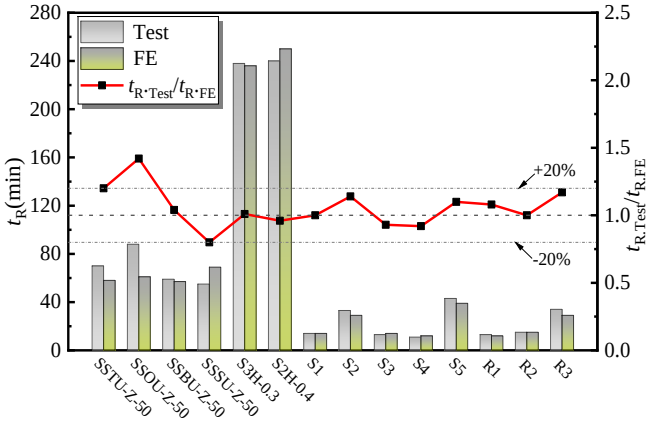

Fig.12 Quantitative comparisons on fire resistance

The demonstrated results indicate that the FE-based model provides good predictions in the overall trend, although some discrepancies occur. The predicted fire resistance, however, is generally lower than that of the test results, particularly for specimens SSOU-Z-50 with an error of 42%. This may be chiefly attributed to the following three issues: (i) an inevitable deviation between empirical thermal properties and real values; (ii) a large dispersion on constitutive models of material at elevated temperature; and (iii) a deviation in initial load eccentricity (as it will be discussed in section 4.3). Despite this, the fire resistance of SRCFST columns subjected to non-uniform fire can be well predicted by the FE-based models developed above. In addition, the failure modes obtained by the FE-based calculations are compared with the observed results, as illustrated in Fig. 13. The graphed results display that the effective simulation of bending and local buckling of SRCFST specimens

could be provided by the FE-based method.

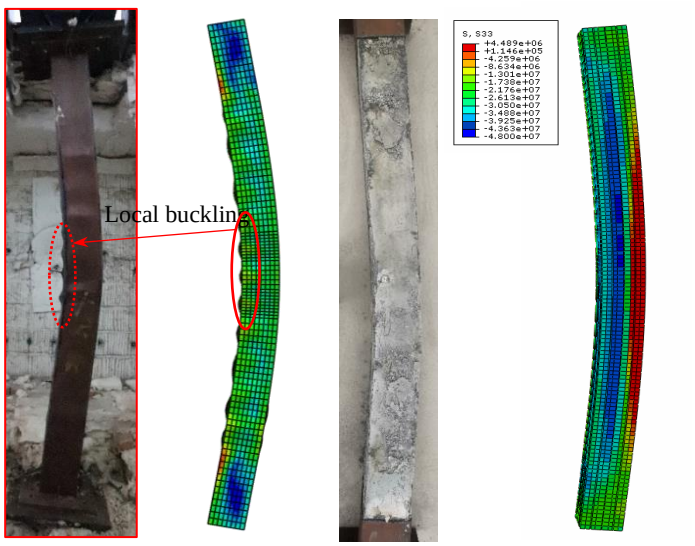

(a) Outer steel tube (b) Infilled concrete

Fig.13 Comparisons of failure modes between the testing and simulated results

4.3 Fire resistance

Based on the verified FE models, the temperature distributions at critical sections of columns are calculated to evaluate the influence of fire boundary on fire behavior of SRCFST columns. Fig. 14 presents the temperature gradients of the critical sections for four test specimens at the end of fire exposure. Compared with the temperature distribution of columns under the uniform fire, some differences between their obtained results are detectable. The temperature gradients are only symmetrically distributed along the X-axis for specimens subjected to 3-face heating and 1-face heating, the low-temperature region shifts towards the unexposed side. Similar to the above, it is diagonally symmetrical for the temperature gradient of the specimen subjected to 2-adjacent-face heating. Therefore, the stiffness center of cross-section is no longer coincident with the geometric center and shifted toward the low-temperature region.

This phenomenon is crucial for the fire performance of columns acted upon by non-uniformly fire, which is in line with previous findings for CFST columns [40]. Therefore, unlike the case of uniform fire, the fire performance of SRCFST columns is influenced by uneven temperature

distribution. These results reveal that: (i) the asymmetric thermal expansion induced by various heating rates generated thermal bowing toward the exposed side, or rather an additional deflection; and (ii) the stiffness center shifts toward the unexposed side during the fire exposure, resulting in an additional load eccentricity.

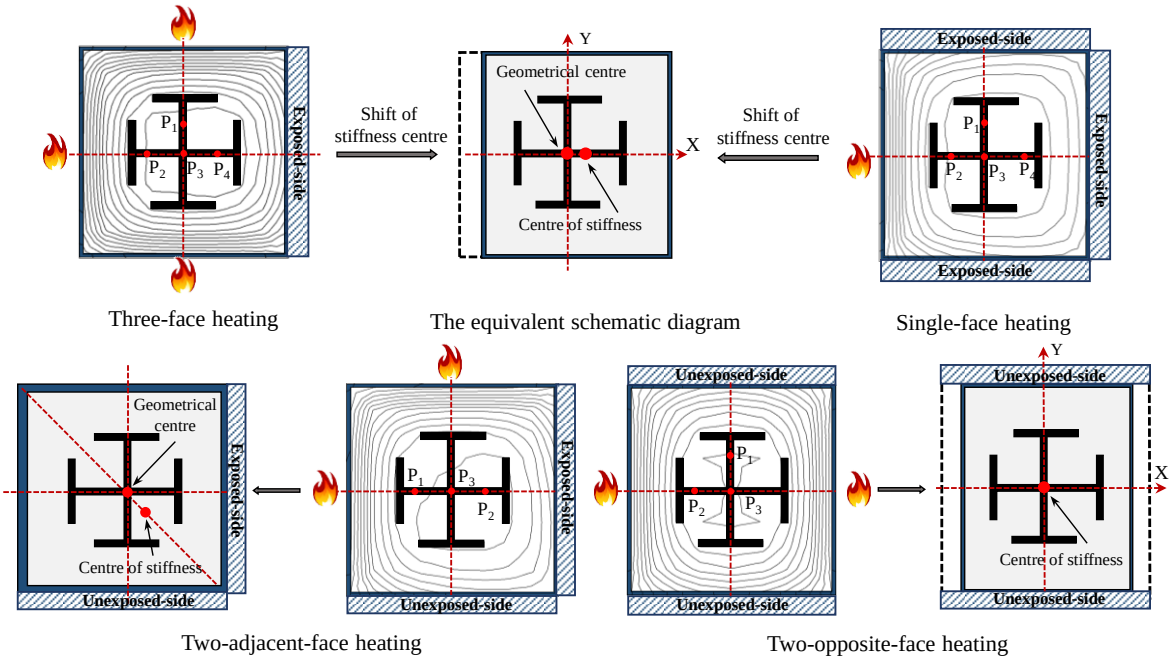

Fig.14 Temperature distribution at the end of fire exposure and corresponding load eccentricities

Based on the asymmetric degradation of stiffness and strength, the cross-sections of columns under 3-, 1-, and 2-opposite-face heating could be considered equivalent to a rectangular, as illustrated in Fig. 14. This results in a change in the loading mode of the column, rather than simply axial compression. For columns subjected to 3-, 1-, and 2-opposite-face heating, the equivalent cross-section has a major and minor axis, and the mechanical behavior of columns subjected to 2-adjacent-face heating can be similar with the columns under biaxial bending.

For axially compressive slender columns, the actual members are not completely straight due to inevitable initial imperfection for columns, such as initial eccentricity or initial deflection. However, the value and direction of load initial eccentricity (near to exposed side and near to unexposed side) cannot be accurately measured prior to the fire resistance test, which have influence on fire resistance

and deflection direction of columns subjected to non-uniform fire. Given the complexity of the non-uniformly applied fire, there are several possible loading positions (P_1 to P_4), as remarked in Fig. 14, in which P_3 is set as ideal axial compression load.

Taking tested specimen in this study as an example, the fire resistance of SRCFST columns under various positions of the initially exerted eccentric load are calculated to further realize the fire behavior of SRCFST columns subjected to the non-uniform fire. Note that load initial eccentricity of $L/1000$ is uniformly assumed to simulate the initial straightness imperfection in FE model. The axially applied load P_3 has been considered for four test specimens in the present paper. The results labeled by FE-$P_{3.1}$ are obtained by applying the initially eccentric load near the P_1, and it can be potentially regarded that the load is applied along the major axis X for specimens under the 3-, 1- and 2-opposite-face heating. Similarly, those labeled FE-$P_{3.2}$ and FE-$P_{3.4}$ are all derived by exerting the initially eccentric load near the P_2 and P_4, respectively.

The fire resistance of SRCFST columns under different loading conditions are calculated and compared in Fig. 15. As stated above, the fire resistance corresponding to FE-$P_{3.1}$ exhibits a maximal level for specimens subjected to 3-, 1-, and 2-opposite-face heating, and is roughly 2 times that of specimens labeled FE-$P_{3.2}$. For SRCFST columns under 3-, 1-, and 2-opposite-face heating, it can be concluded that the columns subjected to eccentric load along the major axis have higher fire resistance. In addition, the fire resistance values based on load model $P_{3.4}$ are commonly higher than those using load model $P_{3.2}$, indicating more adverse of the initial eccentric load toward the exposed side. This fact can be interpreted that the effective centroid of the cross-section shifts toward the unexposed side by the increase of temperature due to asymmetric degradation of material properties. It means that the initial load eccentricity near the exposed side is gradually enlarged during the fire, which is a disadvantage for the fire resistance.

Simultaneously, the deflection direction at the failure may be influenced by the position of the applied load. According to observation on failure mode as shown in Fig. 2, specimen SSTU-Z-50 deflected toward the exposed side, it is contrary to other specimens. Thus, through comprehensive comparisons between both calculated fire resistance and deflection direction and experimental results, the real position of initially eccentric load of four tested specimens can be deducted, as shown in Fig. 15. It is worth mentioning that the fire resistance of SRCFST columns under 3-face heating (SSTU-Z-50) obtained by test is higher than that of SRCFST columns under single-face heating (SSSU-Z-50). Presumably it is because that (1) the position of the initially eccentric load of specimen SSTU-Z-50 is closer to the unexposed side ($P_{3.4}$), which is opposite with that of specimen SSSU-Z-50 ($P_{3.2}$); and (2) the actual initially eccentric load of specimen SSTU-Z-50 may be closer to the effective centroid in fire, or rather closer to the unexposed side than the effective centroid of the section, based on the ultimate direction of bending. In other words, the FE model underestimates the fire resistance of specimen SSTU-Z-50 by assuming an initial load eccentricity of L/1000. This issue also displays the reason for the deviation between the experimental results and the numerically predicted values of the fire resistance.

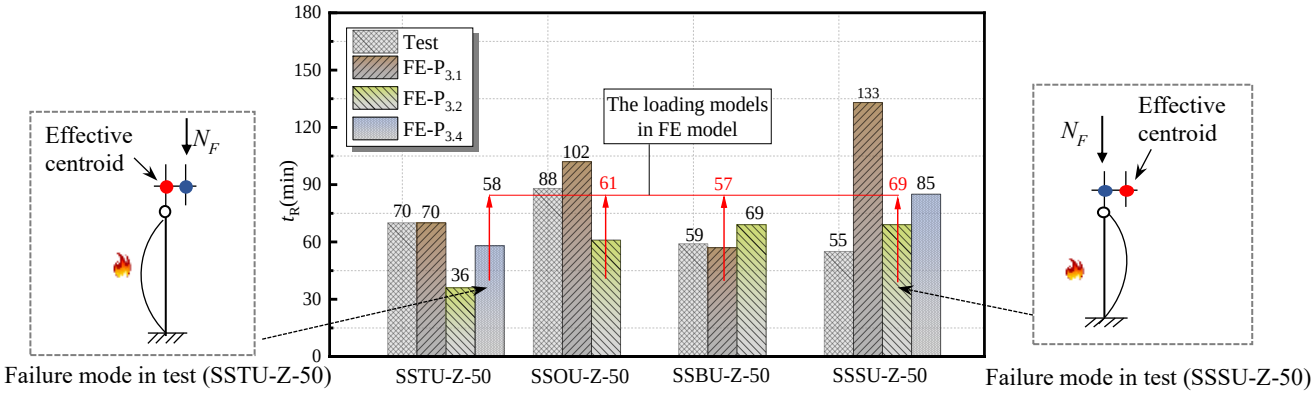

Fig.15 Comparisons on fire resistance of test specimens under different fire conditions

For SRCFST columns under same load conditions, as expected, the columns with fewer exposed sides exhibit a higher fire resistance, as shown in Fig. 15. For SRCFST columns subjected to 1-face

heating, the fire resistance substantially enhances compared to that of other cases subjected to uniform fire. In such a case, an increase ranging from 47% to 177% considering various load conditions is detectable.

4.4 Parametric studies

Based on the above, the main parameters, including load level (n), slenderness ratio (λ), material properties (f_{cu}, f_{ty}, f_{sy}), steel tube ratio (α_{st}, which represents the ratio of the cross-sectional area of the steel tube to that of the concrete), profiled steel ratio (α_{ss}, where denotes the ratio of the cross-sectional area of profiled steel to that of the concrete), sectional dimension (B), and eccentricity ratio (e/r_0) are examined over wide range values to evaluate their effects on the fire resistance under the non-uniform fire. Table 3 summarizes the values of the studied parameters. A total number of 1080 numerical data on fire resistance have been derived. The initial eccentricity of $L/1000$ is imposed at the more adverse position of columns. The eccentricity ratio close to the exposed side is taken as a negative one. The calculated fire resistance demonstrates a similar developed trend for four fire conditions; therefore, the only results for columns under 2-adjacent- and 1-face heating are presented in Fig. 16.

Table 3 Values of studied parameters

Parameter	Values	Fixed value
Load level (n)	0.3, 0.4, 0.5, 0.6, 0.7	0.4
Slenderness ratio (λ)	20, 30, 40, 50, 60, 80	40
Dimension (B)/mm	200, 400, 800, 1000, 1200, 1500	400
Concrete strength (f_{cu})	30, 40, 50, 60	60
Yield strength of steel tube (f_{ty})	235, 355, 390, 420	355
Yield strength of profiled steel (f_{sy})	235, 355, 390, 420	355
Steel tube ratio (α_{st})	0.05, 0.10, 0.15, 0.20	0.1
Profiled steel ratio (α_{ss})	0.04, 0.05, 0.08, 0.10	0.05
Eccentricity ratio (e/r_0)	-0.8~0.8	0

Load ratio (n), sectional dimension (B), and slenderness ratio (λ) have a significant effect on the fire resistance. The fire resistance quickly lessens with the increase in the load ratio, particularly for columns with larger slenderness ratios. The slenderness ratio (λ) also has a negative influence on the fire resistance, which can be attributed to the loss of stiffness. For columns with a larger slenderness

ratio (λ) at high temperatures, more sensitivity to fire resistance is observed, and earlier failure is essentially caused by globe buckling. As expected, the fire resistance of SRCFST columns remarkably enhances with the growth of the sectional dimension (B). It is mainly attributed to the fact that the heat absorption capacity of the cross-section enhances with the increase of the concrete area, which could be represented by the section factor, i.e., A_m/V (m^{-1}) [49]. The results in Figs. 16(d)-(f) reveal that the strength of both steel and concrete trivially affects the fire resistance. The fire resistance of SRCFST columns grows with the increase of profiled steel ratio but lessens for the steel tube ratio. These results readily explain that: (i) the bearing capacity of the steel tube decreases due to the degradation of material properties at elevated temperatures; and (ii) the load shared by the profiled steel enhances with rising temperature due to load redistribution. Therefore, the loss of bearing capacity would be more serious for columns with a larger steel tube ratio, resulting in a negative impact on the fire resistance. Concerning the profiled steel, however, the bearing capacity enhances by increasing the profiled steel ratio because of the limited degradation of the strength. In general, the influence of both steel tube ratio and profiled steel ratio on the fire resistance is limited.

Interestingly, the influence of load eccentricity ratio on the fire resistance of SRCFST columns subjected to non-uniform fire is wholly different from those under the uniform fire, particularly for specimens under 3-, 2-adjacent-, and 1-face heating (see Fig. 17). The obtained results revealed that the fire resistance mutates within a narrow range of eccentricity ratio and peaks at eccentricity ratio of 0.1. It implies that the applied load alignment overlaps with the effective stiffness center at the peak of fire resistance. However, the above phenomenon is not significant for specimens with a slender ratio of 80. In fact, the influence of the second-order effect on the deformation is more noticeable for specimens with a large slender ratio, resulting in more rapid failure. Outside this range, the specimens with eccentricity toward the exposed side ($e/r_0<0$) exhibit a higher fire resistance

compared to those with the same eccentricity but reverse direction (e/r_0>0). The main reason can be explained as follows. For specimens with eccentricity toward the exposure side, thereby the failure is postponed, and the deformation caused by the thermal expansion can be counteracted by reverse deformation induced by the external load. However, the specimens are subjected to eccentricity loads close to the unexposed side and then bend toward the exposed side, resulting in the same directional deflection as the additional one. It could accelerate the global failure of specimens and generate an adverse effect on the fire resistance. Generally, outside the narrow range, the influence of the load eccentricity on the fire resistance of SRCFST columns under the action of non-uniform fire is limited.

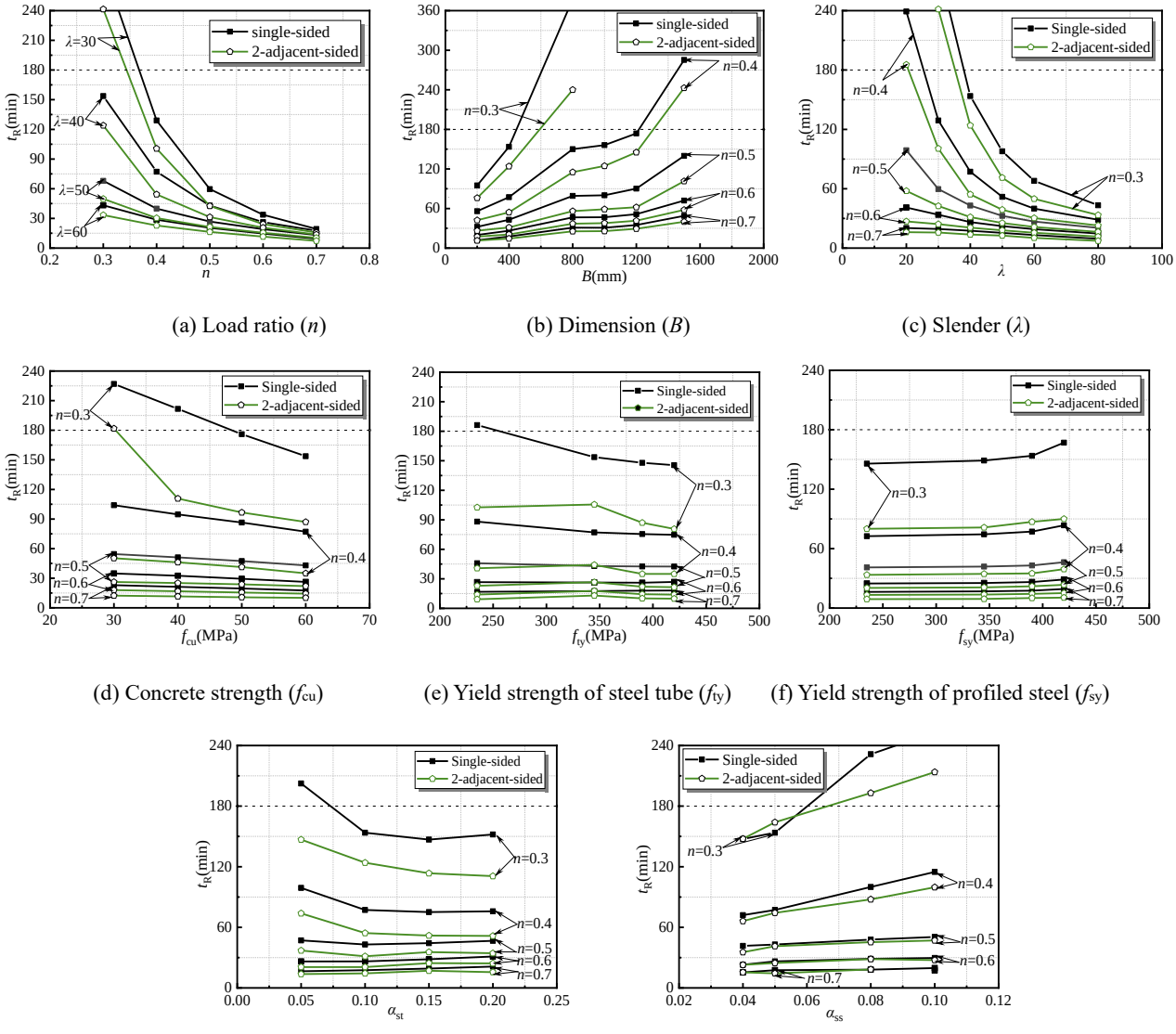

(a) Load ratio (n) (b) Dimension (B) (c) Slender (λ)

(d) Concrete strength (f_{cu}) (e) Yield strength of steel tube (f_{ty}) (f) Yield strength of profiled steel (f_{sy})

(g) Steel tube ratio (α_{st}) (h) Profiled steel ratio (α_{ss})

Fig.16 Effects of key parameters on the fire resistance of SRCFST columns

In general, the parametric results indicate that the fire resistance of SRCFST columns with a low slender ratio (λ<30) can achieve a class I fire resistance rating of 180 min under a low load level (n=0.3). Additionally, SRCFST columns with large dimensions (B>800 mm) which are acted upon by common load levels (n≤0.4) exhibit the fire resistance in the class I category (180 min). In other words, smaller slenderness ratios and larger sectional dimensions are recommended for the fire design of SRCFST columns. It should be noticed that the eccentricity ratio (e/r_0=0.1) associated with the peak fire resistance can only be evaluated by utilizing the parameters given in Table 3. It is recommended that the beneficial effects of the fire resistance within the range of eccentricity ratio are ignored due to the structural-mechanics analysis complexity.

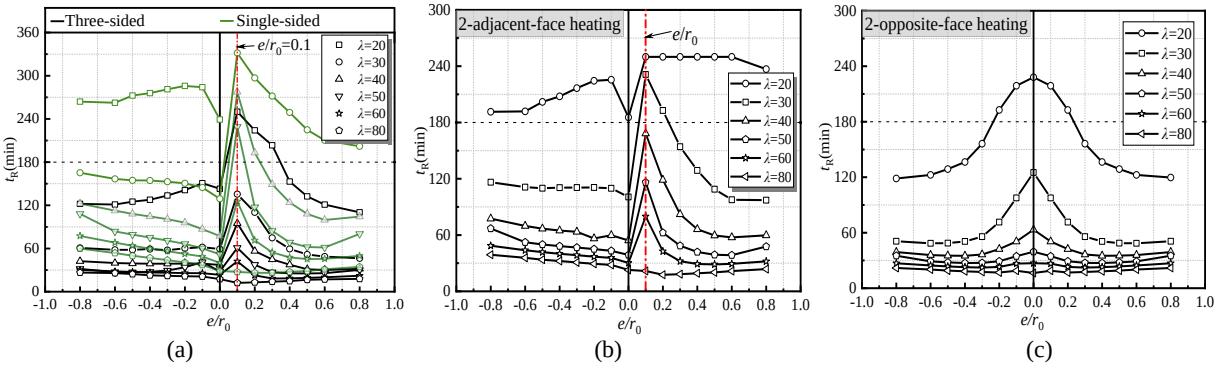

Fig.17 Effects of eccentricity ratio (e/r_0) on the fire resistance of SRCFST columns under the non-uniform fire

5. A simplified method for SRCFST columns

Various design approaches, as set out in Guo et al. [43], Yao et al. [44], EN 1994-1-2 [25], and Tan et al. [54], are recommended to evaluate the ultimate load capacity of CFST columns under the fire. At present, a systematic design methodology for predicting the ultimate load capacity of SRCFST columns subjected to the standard fire (both non-uniform and uniform fire) is still lacking. Herein the simple calculation models in EN 1994-1-2 [25] only are employed for concrete-filled hollow sections (including SRCFST columns) exposed to uniform fire; nevertheless, there is a larger deviation between the predicted fire resistance results and those of test data for SRCFST columns according to Ref. [46]. Additionally, Yao et al. [44] and Tan et al. [54] proposed simplified calculation approaches

to predict the fire resistance of axially and eccentrically loaded CFST columns under the uniform fire via the extended Rankine approach. The given approaches were then further modified by Guo et al. [43] to assess the ultimate load capacity of CFST columns subjected to 3-, 2-adjacent, and 1-face heating. Given the significant contribution of the profiled steel on the fire resistance, the existed design approaches are not applicable to SRCFST columns. Based on this fact, a calculation method is developed using the extended Rankine approach to capture the load capacity of SRCFST columns, covering uniform fire, 3-, 2-opposite-, 2-adjacent-, and 1-face heating.

The total load capacity (p) can be considered as the sum of separate bearing capacities shared by each component [43] referring to the Rankine approach. Considering the contribution of profiled steel, it can be stated in the following form:

$$p = p^{\text{core}} + p^{\text{tube}} + p^{\text{steel}} \tag{2}$$

where the superscript entitled steel, tube, and core indicates the individual contribution of the profiled steel, steel core, and steel tube, respectively.

The load capacity of three components under normal temperatures (i.e., p^{core}, p^{tube}, and p^{steel}) could be evaluated as follows:

$$p^{\text{core}} = \mu_{\text{pr}}^{\text{core}} N_r^{\text{core}}(t)\, p_p^{\text{core}}(0) \tag{3a}$$

$$p^{\text{tube}} = \mu_{\text{pr}}^{\text{tube}} N_r^{\text{tube}}(t)\, p_p^{\text{tube}}(0) \tag{3b}$$

$$p^{\text{steel}} = \mu_{\text{pr}}^{\text{steel}} N_r^{\text{steel}}(t)\, p_p^{\text{steel}}(0) \tag{3c}$$

where $N_r(t)$ represents the revised buckling coefficient at time t taking into consideration the normalized column slenderness ratio, p_p denotes the plastic squashing load, μ_{pr} stands for the plastic reduction factor accounting for the load eccentricity effect. For concrete, it is taken as 1.0 and 0.4 in order for axial and eccentric loads [43]. For steel tube and profiled steel, the term μ_{pr} is defined by Eq. (4) [54] assuming a linear interaction. Therefore,

$$\mu_{\mathrm{pr}}^{\mathrm{tube}}=\frac{1}{1+eA_{\mathrm{sy}}/S_{\mathrm{sy}}} \tag{4a}$$

$$\mu_{\mathrm{pr}}^{\mathrm{steel}}=\frac{1}{1+eA_{\mathrm{ss}}/S_{\mathrm{ss}}} \tag{4b}$$

where e denotes the load eccentricity, the symbol S represents the cross-sectional plastic moment, and A is the cross-sectional area. The subscripts "ss" and "sy" represent the peculiarity related to the profiled steel and steel tube, respectively.

The modified buckling coefficient of concrete at elevated temperatures is given by:

$$N_r^{\mathrm{core}}(t)=\frac{\phi_p^{\mathrm{core}}(t)}{1+[\Lambda_r(t)]^2} \tag{5a}$$

where $\Lambda_r(t)$ is the revised normalized slenderness ratio of the column, which can be essentially controlled by concrete caused by serious softening of the steel tube at rising temperatures:

$$\Lambda_r(t)\cong\Lambda_r^{\mathrm{core}}(t)=\sqrt{\frac{\phi_p^{\mathrm{core}}(t)}{\phi_e^{\mathrm{core}}(t)}}\Lambda_r^{\mathrm{core}}(0) \tag{5b}$$

$$\phi_p^{\mathrm{core}}(t)=\frac{p_p^{\mathrm{core}}(t)}{p_p^{\mathrm{core}}(0)} \tag{5c}$$

$$\phi_e^{\mathrm{core}}(t)=\frac{p_e^{\mathrm{core}}(t)}{p_e^{\mathrm{core}}(0)} \tag{5d}$$

According to previous studies, it can be deduced that $\phi_e^{\mathrm{core}}(t)=\phi_p^{\mathrm{core}}(t)$. Therefore, Eq. (5a) can be equivalent to the following relation:

$$N_r^{\mathrm{core}}(t)=\frac{\phi_p^{\mathrm{core}}(t)}{1+[\Lambda_r{}^{\mathrm{core}}(0)]^2} \tag{6a}$$

$$\Lambda_r^{\mathrm{core}}(0)=\sqrt{\mu_{\mathrm{pr}}^{\mathrm{core}}\cdot\frac{p_p^{\mathrm{core}}(0)}{p_e^{\mathrm{core}}(0)}} \tag{6b}$$

The elastic critical load ($p_e^{\mathrm{core}}(0)$) and the plastic collapse load ($p_p^{\mathrm{core}}(0)$) for concrete at normal temperature are evaluated as:

$$p_e^{\text{core}}(0) = \frac{\pi^2[0.2E_{\text{c}}(0)I_{\text{c}} + E_{\text{ss}}(0)I_{\text{ss}}]}{L_e^2} \tag{7}$$

$$p_p^{\text{core}}(0) = Q_{\text{c}}(0) + Q_{\text{ss}}(0) = 0.85 f_{\text{c}}'(0)A_{\text{c}} + f_{\text{ss}}(0)A_{\text{ss}} \tag{8}$$

where $E_{\text{ss}}(0)$ and $I_{\text{ss}}(0)$ denote the elastic modulus and the second moment of area of the profiled steel at normal temperature, respectively. The factors $f_{\text{ss}}(0)$ and $f_{\text{c}}'(0)$ represent the yield strength of inserted profiled steel and cylinder compressive strength of concrete at ambient temperature, respectively. It is noteworthy that the enhancement of plastic collapse load shared by concrete is considered in Eq. (8) because of the reinforcement provided by cruciform profiled steel to the inner concrete. The plastic collapse load of concrete at any time can be taken into account as follows [54]:

$$p_p^{\text{core}}(t) = \beta_{\text{c}i}(t)Q_{\text{c}}(0) + \beta_{\text{ss}i}(t)Q_{\text{ss}}(0) \tag{9}$$

where $\beta_{\text{c}}(t)$ and $\beta_{\text{ss}}(t)$ represent the strength reduction factor of concrete and profiled steel at time t, respectively. The subscript "i" stands for the fire condition; for instance, "2O" and "2B" in order denote 2-opposite- and 2-adjacent-face heating. The strength reduction factor, $\beta(t)$, can be calculated according to Dotreppe et al. [55] in the following form:

$$\beta_{\text{c}}(t) = \frac{\sum_{i=1}^{n} A_{\text{c}i} f_{\text{c}i}'(t)}{A_{\text{c}} f_{\text{c}}'(0)} \tag{10}$$

Therefore, for the SRCFST column under various fire conditions, the respective regression formulas of the strength reduction factor, $\beta_{\text{c}}(t)$, can be proposed as:

$$\beta_{\text{c}4} = \frac{0.98}{\sqrt{1 + (5t_e^{0.013}A_{\text{c}}^{-0.155})^{A_{\text{c}}^{0.55}}}} \tag{11a}$$

$$\beta_{\text{c}3}(t) = 1.12(\beta_{\text{c}4})^{3A_{\text{c}}^{-0.14}} \tag{11b}$$

$$\beta_{\text{c2O}}(t) = 1.14(\beta_{\text{c}4})^{3A_{\text{c}}^{-0.135}} \tag{11c}$$

$$\beta_{\text{c2B}}(t) = 1.14(\beta_{\text{c}4})^{3A_{\text{c}}^{-0.148}} \tag{11d}$$

$$\beta_{\text{c}1}(t) = 1.14(\beta_{\text{c}4})^{3A_{\text{c}}^{-0.21}} \tag{11e}$$

Eqs. (11a)-(11e) have been developed by implementing the FE-based models described in section 4.1. A total of 540 analyzes have been conducted based on various parameters, including cross-sectional dimensions ranging from 200mm to 1500mm, heating time, and five types of thermal boundary conditions. The temperature of each element should be obtained at least intervals of 10min to guarantee accuracy. The fire exposure time for each column is not less than 3 hours. By considering the effects of the strength degradation of the profiled steel at high temperatures, the following relations are proposed using the FE calculations of the temperature field for various exposure times:

$$\beta_{\mathrm{ss}4}=\frac{1}{\sqrt{1+(0.98t_e^{0.01}\cdot 0.95^{\alpha_{\mathrm{ss}}})A_{\mathrm{c}}^{0.51}}} \tag{12a}$$

$$\beta_{\mathrm{ss}3}(t)=1.004(\beta_{\mathrm{ss}4})^{3A_{\mathrm{c}}^{-0.127}} \tag{12b}$$

$$\beta_{\mathrm{ssO}2}(t)=1.004(\beta_{\mathrm{ss}4})^{3A_{\mathrm{c}}^{-0.135}} \tag{12c}$$

$$\beta_{\mathrm{ssB}2}(t)=1.006(\beta_{\mathrm{ss}4})^{3A_{\mathrm{c}}^{-0.153}} \tag{12d}$$

$$\beta_{\mathrm{ss}1}(t)=1.006(\beta_{\mathrm{ss}4})^{3A_{\mathrm{c}}^{-0.194}} \tag{12e}$$

where the profiled steel ratio (α_{ss}) is taken in the range of 0.04-0.10.

For the steel tube and profiled steel, the corresponding plastic collapse load at the ambient temperature P (i.e., P_p^{tube} (0) and P_p^{steel} (0)) can be respectively obtained by utilizing Eqs. (13) and (14). The time-varying buckling coefficient of the steel tube (N_t^{tube} (t)) and the profiled steel (N_t^{steel} (t)) are also provided by Eqs. (15) and (16), where $k_{\mathrm{y}}^{\mathrm{tube}}$ (t) and $k_{\mathrm{y}}^{\mathrm{steel}}$ (t) take into account the strength degradation of the steel tube and profiled steel at high temperatures (i.e., strength reduction factor against exposure time). For the steel tube, the numerical data of $k_{\mathrm{y}}^{\mathrm{tube}}$ (t) can be obtained using Table 4 through general thermal analysis and liner interpolations [54]. However, for profiled steel, extensive analyzes of the temperature field are conducted, revealing that the temperature in profiled steel depends on the cross-sectional dimensions. Thus, the term $k_{\mathrm{y}}^{\mathrm{steel}}$ (t) should be determined by the predicted temperature using FE-based analysis. Once again, the modified factor of the steel tube under

the non-uniform fire $\beta_{yi}(t)$, depending on the exposure time (t) and dimension (B), are given by Eqs. (17a)- (17c); moreover, it is taken as 1.0 for the column subjected to uniform fire [56]. It is emphasized that the term $\beta_{y2}(t)$ could be employed for the column in the presence of 2-opposite- or 2-adjacent-face heating. Further, Eq. (18) is utilized to determine the empirical factor $\gamma(t)$ [55].

$$p_p^{\text{tube}}(0) = f_{\text{sy}}(0)A_{\text{sy}} \tag{13}$$

$$p_p^{\text{steel}}(0) = f_{\text{ss}}(0)A_{\text{ss}} \tag{14}$$

$$N_r^{\text{tube}}(t) = \frac{\beta_{yi}k_{\text{y}}^{\text{tube}}(t)}{1+[\Lambda_r^{\text{core}}(0)]^2} \tag{15}$$

$$N_r^{\text{steel}}(t) = \frac{\beta_{ssi}k_{\text{y}}^{\text{steel}}(t)}{1+[\Lambda_r^{\text{core}}(0)]^2} \tag{16}$$

$$\beta_{\text{y3}} = [(1-\frac{0.5t_e}{0.05\times\frac{D}{8}+0.1})\gamma(t)]^{-1} \tag{17a}$$

$$\beta_{\text{y2}} = [(1-\frac{0.65t_e}{0.05\times\frac{D}{8}+0.1})\gamma(t)]^{-1} \tag{17b}$$

$$\beta_{\text{y1}} = [(1-\frac{0.85t_e}{0.05\times\frac{D}{8}+0.1})\gamma(t)]^{-1} \tag{17c}$$

$$\begin{aligned} &\gamma(t) = 1-0.3t \qquad for\ \ t \le 0.5h \\ &\gamma(t) = 0.85 \qquad\ \ for\ \ t > 0.5h \end{aligned} \tag{18}$$

Table 4 Strength reduction factor of steel tube

Time t (h)	$k_{\text{y}}^{\text{tube}}(t)$	Time t (h)	$k_{\text{y}}^{\text{tube}}(t)$	Time t (h)	$k_{\text{y}}^{\text{tube}}(t)$
0	1	1.5	0.050	3.0	0.020
0.5	0.371	2.0	0.034	3.5	0.015
1.0	0.065	2.5	0.027	4.0	0.011

Branching from CFST columns, RCFST columns with profiled steel ratio of zero (i.e., α_{ss}=0) could be regarded as CFST columns. For simplicity and accuracy, it should be considered in the calculation method. According to Ref. [43], the effect of the slenderness ratio (λ) on the load capacity could be considered for SRCFST columns by utilizing the profiled steel ratio of zero. For this purpose, a reduction coefficient, which is denoted by α, is introduced to Eq. (2) in the following form:

$$p = (p^{\text{core}} + p^{\text{tube}} + p^{\text{steel}})\alpha \tag{19}$$

$$\alpha = \begin{cases} 0.015\lambda + 0.5 & if\ \alpha > 1 \\ 1 & if\ \alpha \le 1 \\ 1 & \end{cases} \begin{matrix} \\ (\alpha_{ss} = 0) \\ (\alpha_{ss} > 0) \end{matrix} \tag{20}$$

The experimental data of SRCFST columns, including those performed by the authors and Meng et al. [45] are employed to check the calculated results. In addition, the load capacity of CFST columns subjected to 3- and 1-face heating reported by Yang et al. [40] is also predicted. The graphical and quantitative assessments of the ultimate load capacity have been performed by comparing the predicted results and those of experimentally observed data, as reported in Fig. 18 and Table 5. The comparisons generally disclose that there exists a trivial discrepancy between the predicted load capacity and those obtained from the experiment. In general, the developed approach provides accurate and safe predictions on the ultimate load capacity of SRCFST columns under the fire.

Table 5 Comparison of experimental data and theoretical predictions

specimen	Fire condition	Concrete type	e(mm)	N_{cal}(kN)	N_{test}(kN)	N_{cal}/ N_{test}	
SSU-Z-40	4-sided	Steel section	0	2574	2404	1.071	
SSU-Z-50	4-sided	Steel section	0	2759	3000	0.920	Mao *et al.*
SSU-P50-40	4-sided	Steel section	50	1842	1672	1.102	[46]
SSU-P80-40	4-sided	Steel section	80	1712	1500	1.141	
SSTU-Z-50	3-sided	Steel section	0	2855	3000	0.952	
SSOU-Z-50	2-opposite-sided	Steel section	0	2880	3037	0.948	This paper
SSBU-Z-50	2-abjacent-sided	Steel section	0	2902	3140	0.924	
SSSU-Z-50	1-sided	Steel section	0	2979	3097	0.962	
S4H3	4-sided	Steel section	0	2124	2200	0.965	
S4H4	4-sided	Steel section	0	2628	2740	0.959	Meng *et al.*
S3H3	3-sided	Steel section	0	2492	2200	1.133	[45]
S4P3	4-sided	Plain	0	1600	1763	0.908	
S1	3-sided	Plain	0	2731	3186	0.857	
S2	3-sided	Plain	0	2437	2121	1.149	
S3	3-sided	Plain	40	2332	2312	1.009	Yang *et al.*
S4	3-sided	Plain	80	1915	1693	1.131	[40]
S5	1-sided	Plain	0	2223	2977	0.747	
S6	1-sided	Plain	0	2075	1987	1.044	
					Mean	0.999	
					COV	0.108	

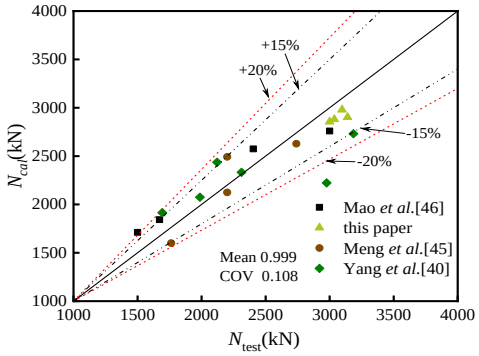

Fig.18 Comparison of theoretical predictions with experimental data on the load capacity

6. Conclusions

Experimental and numerical investigations were conducted to further realize the fire performance of SRCFST columns in the presence of non-uniform fire. The major obtained results are summarized in the following:

(1) All SRCFST specimens under the non-uniform fire presented global buckling accompanied by local buckling of the steel tube. The failure mode of the profiled steel was corresponding to the flexural pattern in overall specimens. The local buckling was observed for the flange of profiled steel at the compression zone. No visible detachment for the interface between the profiled steel and the surrounding concrete was detected, revealing their suitable composite action during the fire exposure.

(2) The fire performance of SRCFST columns was substantially affected by irregular temperature distribution. The lowest temperature regions were closer to the unexposed side, resulting in the stiffness center shifting toward the unexposed side at elevated temperature. Therefore, the asymmetric thermal expansion induced by various heating rates produced thermal bending toward the exposed side. Additionally, the effective centroid of the cross-section shifted toward the unexposed side, causing an additional load eccentricity.

(3) SRCFST columns with fewer sides exposed to fire presented higher fire resistance due to decreasing heat absorption capacity. The axial loading position could have a remarkable effect on the fire resistance of the column exposed to the non-uniformly applied fire. In addition, the maximum value of its fire resistance measure was reported to be about 2 times that obtained by a more adverse load position. The fire resistance of SRCFST columns acted upon by 1-face heating combined with

axial load drastically enhanced compared with that of the case subjected to uniform fire. The obtained results reveal an increase ranging from 47 % to 177 % for various loading positions.

(4) The load ratio, sectional dimension, and slenderness ratio have a substantial influence on fire resistance. The SRCFST columns with low slenderness ratios (λ<30) and common load levels (n≤0.4) exhibit the fire resistance rating in a class I category (180min). The parametric investigations on the eccentricity ratio revealed that the fire resistance abruptly enhanced within the range of the effective centroid of the cross-section, which shifted about 0.05 times the depth toward the unexposed side.

(5) A modified design methodology based on the extended Rankine approach was established to evaluate the ultimate bearing capacity of SRCFST columns under various fire conditions, covering uniform fire, 3-, 2-opposite-, 2-adjacent-, and 1-face heating cases. On the basis of the quantitative comparisons between experiments and predicted results, the developed calculation methodology generally yields accurate and safe prediction results.

Acknowledgements

This work was supported by a grant Nos. 51778274 & 52168020 from National Natural Science Foundation of China.

References

[1] Wang QX, Zhao DZ, Guan P. Experimental study on the strength and ductility of steel tubular columns filled with steel-reinforced concrete. *J Struct Eng* 2004; 130: 1405-1413.

[2] Li GC, Zhan ZC, Yang ZJ, Fang C, Yang Y. Behavior of concrete-filled square steel tubular stub columns stiffened with encased I-section CFRP profile under biaxial bending. *J Constr Steel Res* 2020; 169: 106065.

[3] Chen ZP, Ning F, Song CM, Liang YH. Study on axial compression bearing capacity of novel concrete-filled square steel tube columns. *J Build Eng* 2022; 51: 104298.

[4] Xie WT, Chen Y, Han SH, Zhou WB, He K. Research on I steel reinforced concrete-filled GFRP tubular short columns. *Thin-Walled Struct* 2017; 120: 282-296.

[5] Zhao PT, Huang Y, Liu ZZ, Wang H, Lu YY. Experimental research on seismic performance of

steel fiber-reinforced recycled concrete-filled circular steel tube columns. *J Build Eng* 2022; 54: 104683.

[6] Zhou XH, Yan B, Liu JP. Behavior of square tubed steel reinforced-concrete (SRC) columns under eccentric compression. *Thin-Walled Struct* 2015; 91: 129-138.

[7] Ding FX, Zhang T, Liu XM, Guo Q, Jiang GS. Behavior of steel-reinforced concrete-filled square steel tubular stub columns under axial loading. *Thin-Walled Struct* 2017; 119: 737-748.

[8] Shi YL, Xian W, Wang WD, Li HW. Experimental performance of circular concrete-filled steel tubular members with inner profiled steel under lateral shear load. *Eng Struct* 2019; 201: 109746.

[9] Xian W, Wang WD, Wang R, Chen WS, Hao H. Dynamic response of steel-reinforced concrete-filled circular steel tubular members under lateral impact loads. *Thin-Walled Struct* 2020; 151: 106736.

[10] Qiao QY, Li JF, Mou B, Cao WL. Axial compressive behavior of reinforced concrete-filled stainless steel tube (RCFSST) stub columns: Experimental research. *J Build Eng* 2021; 44: 103431.

[11] Espinos A, Romero ML, Serra E, Hospitaler A. Experimental investigation on the fire behaviour of rectangular and elliptical slender concrete-filled tubular columns. *Thin-Walled Struct* 2015; 93: 137-148.

[12] Espinos A, Romero ML, Serra E, Hospitaler A. Circular and square slender concrete-filled tubular columns under large eccentricities and fire. *J Constr Steel Res* 2015; 110: 90-100.

[13] Romero ML, Moliner V, Espinos A, Ibañez C, Hospitaler A. Fire behavior of axially loaded slender high strength concrete-filled tubular columns. *J Constr Steel Res* 2011; 67: 1953-1965.

[14] Tondini N, Hoang VL, Demonceau JF, Franssen JM. Experimental and numerical investigation of high-strength steel circular columns subjected to fire. *J Constr Steel Res* 2013; 80: 57-81.

[15] Moliner V, Espinos A, Romero ML, Hospitaler A. Fire behavior of eccentrically loaded slender high strength concrete-filled tubular columns. *J Constr Steel Res* 2013; 83: 137-146.

[16] Rodrigues JPC, Laim L. Fire response of restrained composite columns made with concrete-filled

hollow sections under different end-support conditions. *Eng Struct* 2017; 141: 83-96.

[17] Guo Z, Wang X, Zhang XC, Song J, Li CF. Effects of boundary restrains on concrete-filled steel tubular columns with reinforcements exposed to fire. *Thin-Walled Struct* 2019; 142: 52-63.

[18] Ibañez C, Romero ML, Hospitaler A. Fiber beam model for fire response simulation of axially loaded concrete filled steel tubular columns. *Eng Struct* 2013; 56: 182-193.

[19] Wang K, Young B. Fire resistance of concrete-filled high strength steel tubular columns. *Thin-Walled Struct* 2013; 71: 46-56.

[20] Kamil GM, Liang QQ, Hadi MNS. Fiber element simulation of interaction behavior of local and global buckling in axially loaded rectangular concrete-filled steel tubular slender columns under fire exposure. *Thin-Walled Struct* 2019; 145: 106403.

[21] Kamil GM, Liang QQ, Hadi MNS. Numerical analysis of axially loaded rectangular concrete-filled steel tubular short columns at elevated temperatures. *Eng Struct* 2019; 180: 89-102.

[22] Rahnavard R, Craveiro HD, Simões RA, Laím L, Santiago A. Fire resistance of concrete-filled cold-formed steel (CF-CFS) built-up short columns. *J Build Eng* 2022; 48: 103854.

[23] Craveiro HD, Rahnavard R, Henriques J, Simões RA. Structural fire performance of concrete-filled built-up cold-formed steel columns. *Materials* 2022; 15, 2159.

[24] Rahnavard R, Craveiro HD, Simões RA, Santiago A. Equivalent temperature prediction for concrete-filled cold-formed steel (CF-CFS) built-up column sections (part B). *Case Stud Therm Eng* 2022; 35: 102111.

[25] EN 1994-1-2. Design of composite steel and concrete structures-Part 1-2: General rules-Structural fire design: Brussels, Belgium; 2005.

[26] Kodur VKR. Performance-based fire resistance design of concrete-filled steel columns. *J Constr Steel Res* 1999; 51: 21-36.

[27] Hu XX, Guo HC, Yao Y. Interaction approach for concrete filled steel tube columns under fire conditions. *J Build Eng* 2015; 3: 144-154.

[28] Espinos A, Remero ML, Hospitaler A. Simple calculation model for evaluating the fire resistance

of unreinforced concrete filled tubular columns. *Eng Struct* 2012; 42: 231-244.

[29] Yu M, Hu X, Chi Y, Ye JQ. A unified method for calculating the fire resistance of concrete-filled steel tube with fire protection under combined loading. *J Constr Steel Res* 2020; 168: 106003.

[30] Yu M, Hu X, Xu LH, Cheng SS. A general unified method for calculating fire resistance of CFST columns considering various types of steel and concrete. *J Build Eng* 2022; 59: 105125.

[31] Shao ZW, Zha XX, Wan CY. Design method of fire-resistance capacity of reinforced-concrete-filled steel tube column under axial compression. *Fire Saf J* 2022; 129: 103572.

[32] Espinos A, Remero ML, Lam D. Fire performance of innovative steel-concrete composite columns using high strength steels. *Thin-Walled Struct* 2016; 106: 113-128.

[33] Chu TB, Gernay T, Dotreppe JC, Franssen JM. Steel hollow columns with an internal profiled filled with self-compacting concrete under fire conditions. Proceedings of the Romanian Academy Series a-Mathematics Physics Technical Sciences Information Science 2016; 17(2): 152-159.

[34] Yang JJ, Liu JP, Wang S, Wang WY. Experimental and analytical investigation on fire resistance of circular tubed steel reinforced concrete medium-long columns. *J Build Eng* 2021; 44: 102968.

[35] Neuenschwander M, Knobloch M, Fontana M. ISO standard fire tests of concrete-filled steel tube columns with solid steel core. *J Struct Eng* 2017; 143(4): 04016211.

[36] Neuenschwander M, Knobloch M, Fontana M. Modeling thermo-mechanical behavior of concrete-filled steel tube columns with solid steel core subjected to fire. *Eng Struct* 2017; 136: 180-193.

[37] Tan QH, Gardner L, Han LH, Song TY. Fire performance of steel reinforced concrete-filled stainless steel tubular columns with square cross-sections. *Thin-Walled Struct* 2019; 143: 106197.

[38] Yang X, Tang C, Chen Y, Qiao TY. Compressive behavior of steel-reinforced concrete-filled square steel tubular stub columns after exposure to elevated temperature. *Eng Struct* 2020; 204: 110048.

[39] Meng FQ, Zhu MC, Mou B, He BJ. Residual strength of steel-reinforced concrete-filled square

steel tubular (SRCFST) stub columns after exposure to ISO-834 standard fire. *Int J Steel Struct* 2019; 19(3): 850-866.

[40] Yang H, Liu FQ, Zhang SM, Lv XT. Experimental investigation of concrete-filled square hollow section columns subjected to non-uniform exposure. *Eng Struct* 2013; 48: 292-312.

[41] Yang H, Liu FQ, Gardner L. Performance of concrete-filled RHS columns exposed to fire on 3 sides. *Eng Struct* 2013; 56: 1986-2004.

[42] Lyu XT, Zhang T, Liu FQ, Liu YJ. Behaviours of stiffened concrete-filled thin-walled square steel tubular stub columns after non-uniform fire exposure. *J Constr Steel Res* 2022; 188: 107031.

[43] Guo HC, Long X, Yao Y. Fire resistance of concrete filled steel tube columns subjected to non-uniform heating. *J Constr Steel Res* 2017; 128: 542-554.

[44] Yao Y, Liu MJ, Guo HC. Concrete filled double skin steel tubular columns subjected to non-uniform heating. *J Constr Steel Res* 2019; 158: 263-278.

[45] Meng FQ, Zhu MC, Clifton GC, Ukanwa KU, Lim JBP. Performance of square steel-reinforced concrete-filled steel tubular columns subject to non-uniform fire. *J Constr Steel Res* 2020; 166: 105909.

[46] Mao WJ, Wang WD, Zhou K, Du EF. Experimental study on steel-reinforced concrete-filled steel tubular columns under the fire. *J Constr Steel Res* 2021; 185: 106867.

[47] ISO 834-1: 1999. Fire-resistance tests-elements of building construction-Part 1: General requirements. International organization for standardization, Geneva; 1999.

[48] EN 1991-1-2. Actions on structures-Part 1-2: General rules-Actions on structures exposed to fire: Brussels, Belgium; 2002.

[49] Mao WJ, Wang WD, Xian W. Numerical analysis on fire performance of steel-reinforced concrete-filled steel tubular columns with square cross-section. *Struct* 2020; 28: 1-16.

[50] Lu H, Zhao XL, Han LH. FE modelling and fire resistance design of concrete filled double skin tubular columns. *J Constr Steel Res* 2011; 67: 1733-1748.

[51] Lie TT. Fire resistance of circular steel columns filled with bar-reinforced concrete [J]. *J Struct Eng* 1994; 120(5): 1489-1509.

[52] Han LH. Concrete filled steel tubular structures-Theory and practice. 2016, 3rd ed.; Science press, Beijing, China.

[53] Hong S, Varma AH. Analytical modeling of the standard fire behavior of loaded CFT columns [J]. *J Constr Steel Res* 2009; 65(1):54-69.

[54] Tan KH, Tang CY. Interaction model for unprotected concrete filled steel columns under standard fire conditions. *J Struct Res* 2015; 112: 282-292.

[55] Dotreppe JC, Franssen JM, Vanderzeypen Y. Calculation method for design of reinforced concrete columns under fire conditions. *Struct J* 1999; 96: 9-18.

[56] Tan KH, Yao Y. Fire resistance of reinforced concrete columns subjected to 1-, 2-, and 3-face heating. *J Struct Eng* 2004; 130: 1820-1828.